Identification of targetable epigenetic vulnerabilities in uveal melanoma

Gulum Yenisehirli[1,2], Sebastian Borges[1,2], Steffanie S. Braun[1,2], Ashley N. Zuniga[1,2], Gabriela I. Quintana[1,2], Jeffim N. Kutsnetsoff[1,2], Sara Rodriguez[1,2], Emily V. Adis[1,2], Sofia Lopez[1,2], James J. Dollar[1,2], Vasileios Stathias[1], Claude H. Volmar[3,4], Efe Karaca[1,5], Shaun Brothers[3,4], Daniel Bilbao[1,5], J. William Harbour[6], Zelia M. Correa[1,2], Stefan Kurtenbach*[1,2]

[1] Department of Ophthalmology and Sylvester Comprehensive Cancer Center, University of Miami Miller School of Medicine

[2] Interdisciplinary Stem Cell Institute (ISCI), University of Miami Miller School of Medicine

[3] Center for Therapeutic Innovation, University of Miami Miller School of Medicine

[4] Department of Psychiatry and Behavioral Sciences, University of Miami Miller School of Medicine

[5] Department of Pathology and Laboratory Medicine, University of Miami Miller School of Medicine

[6] Department of Ophthalmology and Harold C. Simmons Comprehensive Cancer Center, University of Texas Southwestern Medical Center

*Corresponding author: Stefan Kurtenbach, Department of Ophthalmology, Biomedical Research Building Room 9131501 NW 10th Avenue, Miami, FL 33136, 305-243-3892. sxk321@miami.edu

The authors declare no conflicts of interest.

ABSTRACT

Uveal melanoma (UM) is the most prevalent primary intraocular malignancy in adults, which preferentially metastasizes to the liver in approximately half of all cases. Metastatic UM is notoriously resistant to therapy and is almost uniformly fatal. UM metastasis is most strongly associated with mutational inactivation of the *BAP1* tumor suppressor gene. Given the role of BAP1 in epigenetic regulation as the ubiquitin hydrolase subunit of the polycomb repressive deubiquitinase (PR-DUB) complex, we conducted high-throughput drug screening using a well-characterized epigenetic compound library to identify new therapeutic vulnerabilities. We identified several promising new lead compounds, in particular the extra-terminal domain protein (BET) inhibitor mivebresib (ABBV-075). Mivebresib significantly improved survival rates in a metastatic uveal melanoma xenograft mouse model and entirely prevented detectable metastases to the bones, spinal cord, and brain. RNA sequencing revealed a notable overlap between the genes and pathways affected by HDAC and BET inhibition, including the reversal of gene signatures linked to high metastatic risk and upregulation of genes associated with a neuronal phenotype. Together, we found that UM cells are particularly vulnerable to class I HDAC and BET inhibition, and highlight the BET inhibitor mivebresib as a promising candidate for further clinical evaluation.

INTRODUCTION

Uveal melanoma (UM) is the most prevalent primary intraocular malignancy in adults, with metastases occurring in approximately half of all cases. UM metastases are highly resistant to treatment and almost uniformly lethal (1). Currently, the only FDA-approved treatment for metastatic UM is tebentafusp-tebn (Kimmtrak, Immunocore Limited), a bispecific gp100 peptide-HLA-directed CD3 T-cell engager. However, this treatment is only available for HLA-A*02:01-positive patients and only increases the average life expectancy by months (2). Despite this development being a significant advancement, additional treatment strategies are urgently needed.

UM has a low mutational burden, with a mutational profile distinct from that of cutaneous and other melanomas (3). Mutually exclusive mutations in the Gq signaling pathway, most commonly in *GNAQ* or *GNA11* (4, 5), and less frequently in *PLCB4* (6) and *CYSLTR2* (7), are present in virtually all UMs (8), but also in benign ocular nevi (4, 5, 8, 9). Therefore, these mutations alone are insufficient for malignant transformation. Additional secondary mutations in either *BAP1* (10), *SF3B1* (11), or *EIF1AX* (12) ('BSE' mutations) occur in a mutually exclusive manner and are associated with high, medium, and low metastatic risk respectively (13-15). Hence, *BAP1* mutations are among the most significant clinical markers of high metastatic risk in patients with UM. Mutations in *BAP1* result in the loss of BAP1 function and are usually accompanied by the loss of one copy of chromosome 3, where *BAP1* is located, resulting in complete loss of BAP1 activity (10). BAP1 is a ubiquitin carboxy-terminal hydrolase that acts as the catalytic subunit of the polycomb repressive deubiquitinase complex (PR-DUB), which opposes PRC1 activity by removing transcriptionally repressive monoubiquitin marks from histone H2AK119 (16-18). BAP1 depletion in various cell and animal models leads to global changes in H2AK119 ubiquitination and

the epigenome (19, 20). BAP1 loss also leads to the failure of the H3K27ac histone mark to accumulate at the promoter sites of key lineage commitment genes, highlighting its role in the broader regulation of transcription and cell differentiation (19).

Given the epigenetic changes in metastatic UM (21), we conducted high-throughput screening of epigenetically active, small-molecule modulators to target UM. We identified several compounds that potently reduced UM cell viability *in vitro*, including the FDA-approved class I histone deacetylase (HDAC) inhibitor romidepsin, and the bromodomain and extra-terminal domain protein (BET) inhibitor mivebresib. Further, mivebresib significantly inhibited metastasis *in vivo* in a mouse model of UM.

METHODS

Cell culture. UM (MP41, MP46, and MP38) cell line stocks were obtained from the American Type Tissue Collection (ATCC). UM cells were cultured at 37°C under normoxic conditions (5.0% CO_2, 5% O_2) in D-MEM/F-12 medium with 10% heat-inactivated FBS, 2 mmol/L GlutaMAX, 1 mmol/L Non-Essential Amino Acid (NEAA) cell culture supplement, 0.5 × Insulin-Transferin-Selenium (ITS), and 1x Pen-Strep (10,000 U/mL, Gibco). All the UM cell lines were verified using STR analysis.

Compound screening. For the primary screening, we tested a 932-compound epigenetic library (TargetMol, L1200) consisting of inhibitors and activators of epigenetic-modifying enzymes (writers, erasers, and readers). All stock compounds were dissolved in 100% DMSO and tested in duplicates at a final test concentration of 1 µM and a final DMSO concentration of 0.1% of DMSO. Wells with assay buffer (HBSS) containing 0.1% DMSO served as negative controls. Velcade (10 µM bortezomib) served as the positive control. One thousand cells per well were seeded in 384-well white microtiter plates in a humidified incubator at 37°C with 5% O_2 and 5% CO_2 overnight (~16 h). The cells were then treated with these compounds for 72 h. Cell viability was assessed by measuring ATP levels using a luminescence-based assay (CellTiter-Glo, Promega) on a Perkin Elmer Envision Multilabel Plate Reader. Positive hits were defined as compounds that showed cell death higher than the mean of the negative controls plus 3 standard deviations. Assays on each plate were considered valid only when the Z'-factor of the plate was equal to or greater than 0.5 ($Z' \geq 0.5$).

Concentration-response testing. Cell lines were treated using a 10-point 1:3 dilution series starting at a nominal test concentration of 10 µM for all drugs, except romidepsin, for which the starting concentration was 300 nM (n =4, 20,000-fold concentration range). Cell viability was assessed after 72 h of treatment by measuring ATP levels using a luminescence-based assay (CellTiter-Glo, Promega) on a Perkin Elmer Envision Multilabel Plate Reader, and normalized to the viability of cells treated with 0.1% DMSO, which served as the negative control. Four-parameter curve fitting (non-linear regression, log(inhibitor) vs. response, variable slope) performed using GraphPad Prism to measure the efficacy (% cell viability) and potency (IC_{50}) of each compound.

Animal studies. The University of Miami Institutional Animal Care and Use Committee (IACUC) approved all animal procedures. Female NOD Scid Gamma (NSG) mice were obtained from Jackson Laboratory (Stock No.

002374) and bred in-house for one generation. MP41 cells were transduced with retroviruses expressing RFP-luciferase (pMSCV-IRES-luciferase-RFP), and successful transduction was confirmed by imaging the cells on a cell imager (Zoe, Bio-Rad, Hercules, CA, USA) with an RFP filter. After transduction, RFP-positive cells were sorted and purified using FACS. For the model generation, 1 × 105 cells were injected intravenously (tail vein) into 16-week-old female NSG mice (n = 10 per group). Treatment groups assignments were randomized.The development of tumor metastasis was monitored weekly during the course of the experiment using an in vivo imaging system (IVIS Spectrum, Revvity). Briefly, 10 min prior to imaging, mice were injected intraperitoneally with d-luciferin (Perkin Elmer #760504) at a dose of 150 mg/kg. Mice were sacrificed at the endpoint (defined as more than 20% weight loss or significant changes in health status), and tumor metastases in different organs were quantified ex vivo using IVIS. Significance testing for survival curves were conducted with the log-rank (Mantel-Cox) test.

Isolation of mouse liver metastatic cells. Tumor-bearing liver tissue was minced and incubated in collagenase Type IV solution (1x D-MEM with 400 U/mL Type IV collagenase powder (Gibco) and 0.5 µg/mL Amphotericin B solution (Sigma)) overnight at 4°C. The next day, tumor cells from the liver were grown in UM media (see above) and confirmed to be MP41 cells by RFP fluorescence.

RNA sequencing. For the 24-hour treatment RNA-seq analysis, 100,000 cells were seeded per well in 6-well plates in triplicate for each treatment group. 24 hours after seeding, cells were treated with romidepsin (40 nM), quisinostat (40 nM), or mivebresib (1200 nM). Concentrations were chosen through initial testing and doses that elicited a morphological change without successive cell death were selected. Wells treated with 0.1% DMSO served as the control group. Total RNA was extracted 24 h after treatment using the Zymo Research Quick-RNA MiniPrep kit and the samples were sequenced by BGI (Cambridge, MA, USA). All samples were sequenced with over 18 million paired-end reads (150 base pairs). The treatment group files were concatenated and analyzed using BioJupies, which utilizes *limma* powered differential expression analysis (22). Pathway analysis was performed with Metascape using significantly differentially expressed genes (Adj. $P < 0.05$, $\log_2 FC > |1.5|$) (23) and transcription factor analysis was performed using ChIP Enrichment Analysis (ChEA) (24). Data will be available on the Gene Expression Omnibus(GEO) data repository upon publication.

iLINCS analysis. To compare the transcriptomic changes caused by our drugs to other perturbations, we used the Library of Integrated Network-based Cellular Signatures (iLINCS) (25) data portal to identify genes dysregulated by HDAC treatments. We identified 180 genes that were consistently up- or down-regulated as a result of treatment with 8 different HDAC treatments (trichostatin A, vorinostat, panobinostat, dacinostat, romidepsin, belinostat, entinostat, mocetinostat) across analyzed cell lines, and determined the gene expression shifts of these genes as a result of HDAC and BET inhibitor treatment in our cell lines. We additionally used the connected perturbations analysis function of iLINCS to identify compounds eliciting gene signatures similar to those in our study using lists of significantly differentially expressed genes (Adj. $P < 0.05$, $\log_2 FC > |1.5|$).

RESULTS

Epigenetic compound screening identifies new vulnerabilities in UM

Given the epigenetic changes correlating with metastatic spread in UM, we performed a comprehensive screeni of epigenetic compounds to explore new potential vulnerabilities. We utilized a well-characterized, epigenetically active compound library consisting of 932 potent, cell-permeable small-molecule modulators (TargetMol, L1200), many of which are FDA-approved. We tested this library on two *BAP1*-mutant UM cell lines (MP38 and MP46), as well as one *BAP1*-wildtype cell line (MP41) (26). The initial screen proved to be very specific and identified 24 compounds that significantly reduced cell viability in at least one cell line at 1 μM and 72 h of treatment (n = 2 per compound) (fig. 1A). Most of the drug classes in the compound library had low efficacy against the UM cell lines, including histone methyltransferase inhibitors (17% of compounds tested (n = 160), 0% hits), histone acetyltransferase inhibitors (7% of compounds tested (n = 68), 0% of hits), and ataxin inhibitors (18% of compounds tested (n = 167), 8% of hits (n = 2)) (fig. 1B, 1C). BET inhibitors, which accounted for only 4% of the compound library (n = 36), comprised 29% of the hits (n = 7). HDAC inhibitors accounted for 7% of the compounds tested (n = 64), but 25% of the hits (n = 6). Poly ADP Ribose Polymerase (PARP) inhibitors (n = 28) did not significantly reduce cell viability in these three cell lines (fig. 1B, supplemental fig. 1A).

Twenty-one of the most promising compounds in comprehensive concentration-response regimens were tested (10 concentrations, n = 4) (g. 1D, Supplemental Table 1), and 18 of the compounds had IC_{50} values of less than 1 μM. The HDAC inhibitor romidepsin had the highest potency in all UM cell lines ($IC_{50} \approx 3.5$ nM), even lower than that of Velcade ($IC_{50} \approx 7.6$ nM), a highly potent and cytotoxic proteasome inhibitor (27) that was used as a positive control in this screen. Individual compounds had similar IC_{50} values for the three cell lines tested, despite their genetic differences, namely MP41 being *BAP1*-wildtype and MP38 and MP46 being *BAP1*-mutant (fig. 1E, 1F).

Of the 18 compounds with an IC_{50} of less than 1 μM, 13 were either HDAC or BET inhibitors, and only five compounds targeted other mechanisms. Gemcitabine ($IC_{50} \approx 493$ nM), a DNA synthesis inhibitor (28) that demonstrated synergistic activity with treosulfan in phase II clinical trials for metastatic UM (29), and staurosporine ($IC_{50} \approx 336$ nM), a broad kinase inhibitor (30), have previously been shown to induce apoptosis in UM cells (31, 32). Camptothecin ($IC_{50} \approx 334$ nM) (topoisomerase I inhibitor (33)), podofilox ($IC_{50} \approx 9.36$ nM) (microtubule destabilizer (34)) and cucurbitacin B ($IC_{50} \approx 37.9$ nM) (inhibitor of AKT, HIF1a, and STAT3 (35)), to our knowledge, have not previously been tested for UM. We further tested for synergy between romidepsin and quisinostat with the other 16 compounds. However, despite these compounds targeting diverse epigenetic pathways, none synergized significantly (supplemental fig. 2).

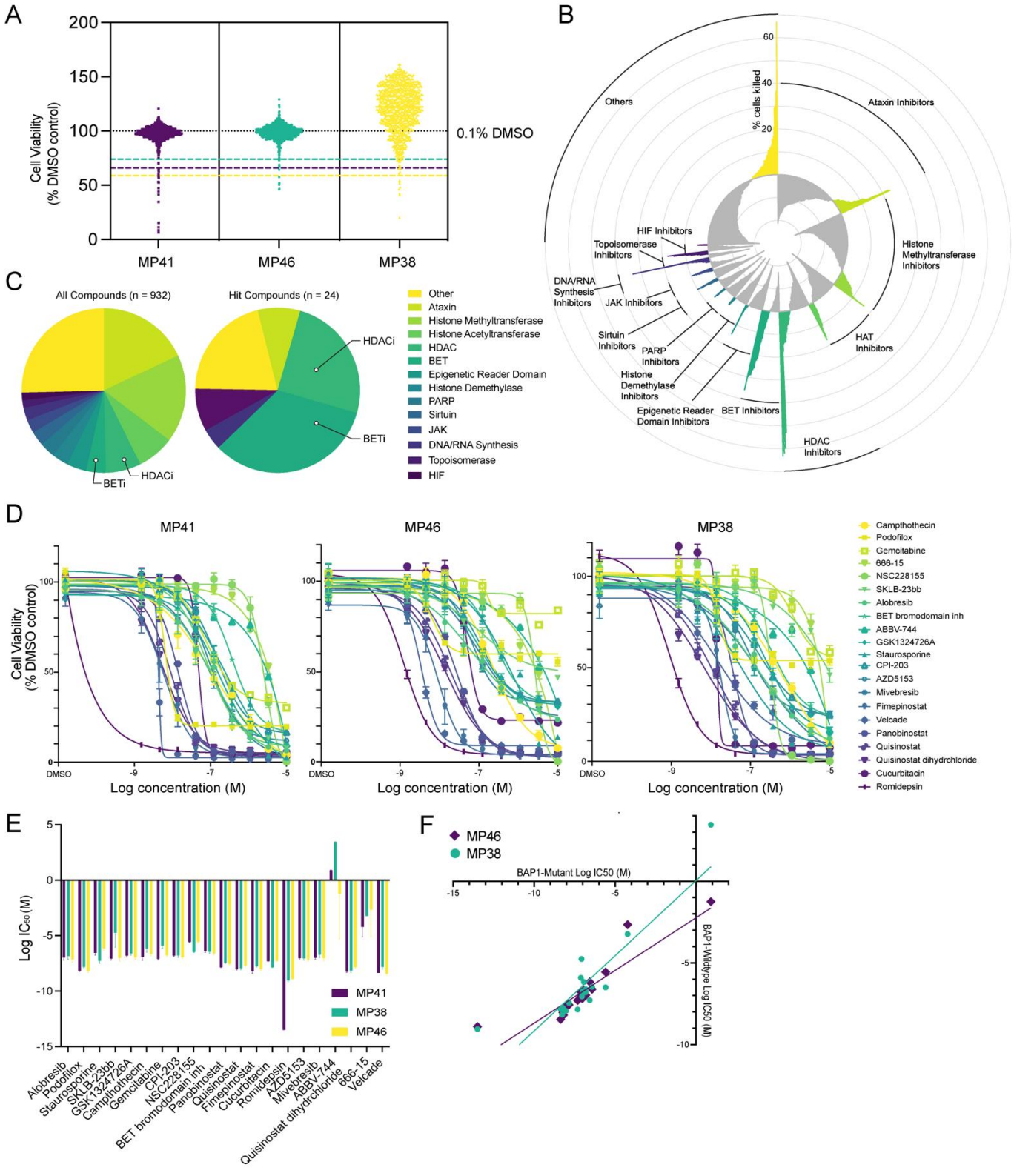

Figure 1. Primary screening for epigenetic compounds in UM cells. (A) Viability of the three UM cell lines following treatment with 932 epigenetic modulators at a concentration of 1 μM (n = 2). Hit cut-offs (dashed lines) were determined as the mean of the negative controls minus three standard deviations. **(B)** Radar plot showing the average percentage of cell death for the three cell lines treated with 932 compounds. **(C)** Pie charts of the molecular activities of all screened compounds (left) and the hits identified (right). **(D)** Dose-response experiments for the identified compounds (10 concentrations, n = 4 per concentration per cell line). **(E)** $LogIC_{50}$ values of the top-hit compounds for each cell line. Error bars represent 95% confidence interval. **(F)** $LogIC_{50}$ of BAP1 mutant cell lines (MP46 and MP38) plotted on the X-axis against the $LogIC_{50}$ of the BAP1 WT cell line (MP41) on the Y-axis.

HDAC inhibition in uveal melanoma cells

HDAC inhibition has been used in numerous studies and clinical trials on UM (36-43). However, there are 11 HDAC isoforms that function in numerous protein complexes and have diverse biological functions (44-46), and it is unclear which HDACs are the most promising to specifically target in UM. Romidepsin demonstrated the greatest potency *in vitro*, suggesting that inhibition of class I HDACs may be a vulnerability for UM, as Romidepsin specifically inhibits class I HDACs (HDAC1, 2, 3, and 8). Although no specific inhibitors of HDAC1 and HDAC2 exist, we tested the HDAC3 inhibitor RGFP966 (TargetMol, T1762) and the HDAC8 inhibitor PCI-34051 (TargetMol, T6325) and found that neither was potent in *BAP1*-wildtype or *BAP1*-mutant cell lines, either alone or in combination (fupplemental fig. 1B). We tested romidepsin from two different sources (TargetMol T6006, Sigma SML1175) and included an additional primary *BAP1*-mutant UM cell line we generated (UMM66) (fig. 2A). Both Romidepsin batches showed similar potency in all UM cell lines, including UMM66 cells (IC_{50} = 2.4 - 5.7 nM). Together, these data highlight romidepsin as the most potent compound in this *in vitro* screen, and the specific inhibition of class I HDACs, likely acting through HDAC1 and/or HDAC2, as a potential vulnerability of UM.

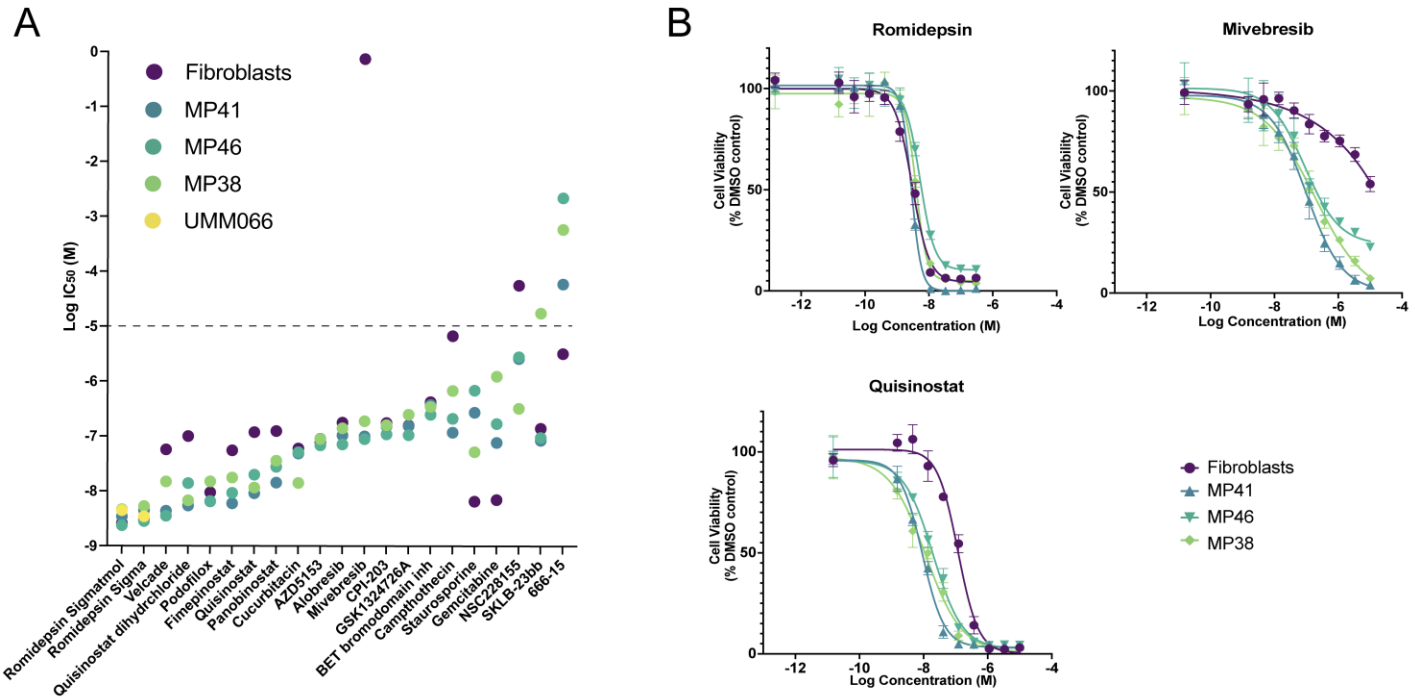

Figure 2. IC_{50} and dose-response curves of lead candidates in UM cell lines versus normal fibroblasts. (A) $LogIC_{50}$ values of the lead compounds in UM cell lines and normal fibroblasts. The dotted line indicates the highest concentration of drug used (10 μM); hence, for the values above, the IC_{50} is not determined accurately. n = 4 replicates for each concentration were tested. **(B)** Concentration-response curves of the top candidates (romidepsin, mivebresib, and quisinostat) for UM cell lines and WS1 fibroblasts. n = 4 per concentrations tested.

BET inhibition in uveal melanoma cells

To explore the non-specific toxicities of the identified compounds, we performed viability assays on a non-cancerous WS1 fibroblast cell line. The HDAC inhibitors fimepinostat (fibroblast $IC_{50} \approx 55$ nM, UM $IC_{50} \approx 11$ nM) and panobinostat (fibroblast $IC_{50} \approx$ 124 nM, UM $IC_{50} \approx 26$ nM) demonstrated 4- to 5-fold lower toxicity to non-transformed cells. Quisinostat had an approximately 9 times higher IC_{50} for non-cancerous cells on average (fibroblast $IC_{50} \approx 118$ nM) than for UM cells (UM $IC_{50} \approx 14$ nM) (fig. 2A). Other drugs with lower cytotoxicity to normal cells included velcade (fibroblast $IC_{50} \approx 57$ nM, UM $IC_{50} \approx 8$ nM) and campthothecin (fibroblast $IC_{50} \approx 7$ µM, UM $IC_{50} \approx 334$ nM). Of particular interest, the BET inhibitor mivebresib showed minimal toxicity to normal fibroblasts ($IC_{50} > 10$ µM), while being potent in UM cell lines ($IC_{50} \approx 125$ nM).

Although the primary treatment of UM with radiation or enucleation has a high rate of tumor control, approximately half of all patients develop fatal metastases. Therefore, we tested our lead compounds in a mouse model of UM to determine their ability to reduce metastatic growth. Initially, we tested various UM cell lines and found that MP41 cells readily metastasized predominantly to the liver when injected into the tail vein. MP41 is *BAP1*-wildtype, and was derived from an aggressive UM case that had spread to multiple organs and has features of *BAP1*-mutant UM, including the loss of one copy of chromosome 3 (monosomy 3) (47). As we did not find significant differences between MP41 and the *BAP1*-mutant cell lines MP46 and MP38 regarding drug sensitivity, we deemed this model, which recapitulates the hematogenous spread and liver invasion in humans, as most suitable to explore the inhibition of metastatic growth with the lead compounds.

We labeled MP41 cells with luciferase for *in vivo* monitoring and *ex vivo* testing of organs for metastatic disease. Seven days after cell injection, drug treatments were initiated to determine the efficacy of each treatment in slowing metastatic growth. Toxicity assays were conducted prior to determine optimal drug doses, which were 2 mg/kg of romidepsin via weekly intraperitoneal (IP) injection, 5 mg/kg of quisinostat five times per week via IP injection, and 2 mg/kg of mivebresib five times per week via oral gavage (fig. 3A). Quisinostat and romidepsin treatments did not significantly improve survival rates in comparison with the vehicle group ($p > 0.10$) in this metastatic mouse model, with median survival rates between 83-88.5 days after tumor cell inoculation (fig. 3B). Mivebresib treatment significantly increased median survival to 120.5 days ($p = 0.01$). *Ex vivo* IVIS imaging revealed that mivebresib prevented metastasis to the femur, which was detected in all other experimental groups (vehicle, n = 4; romidepsin, n = 2; quisinostat, n = 4) (fig. 3C, 3D). Mivebresib further prevented spinal cord metastases that were present in the other groups (vehicle, n = 5; romidepsin, n = 2; quisinostat, n = 4) (fig. 3C, 3D).

To test whether long-term treatment of mice led to UM metastasis developing resistance towards the compounds, we extracted UM cells from liver metastases from all treatment groups and performed concentration-response testing. No significant resistance was detected in any of the treatment groups relative to that in the vehicle-treated group (supplemental fig. 3).

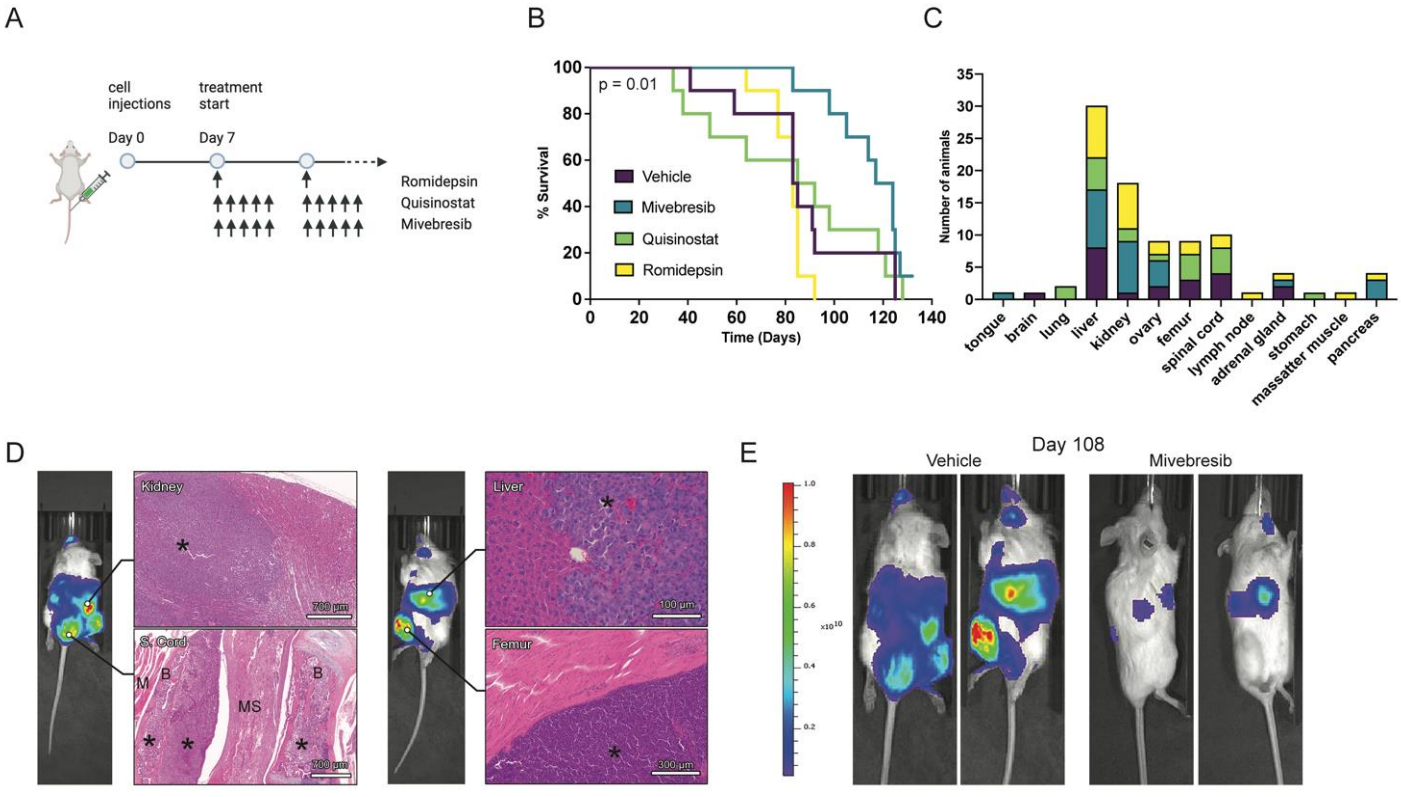

Figure 3. BET inhibition reduces metastatic UM growth *in vivo*. (A) Mouse model and timeline of the UM metastatic mouse model. **(B)** Survival of mice in each treatment group (n = 10 per group). **(C)** Sites of metastasis. The number of mice with metastatic foci in each organ per treatment are shown. **(D)** Representative histopathological images of kidney, spinal cord (S. cord), liver, and femur metastases from the vehicle-treated group. (* = tumor cells; M = muscle; B = bone; MS = medulla spinalis). **(E)** Representative IVIS images of the vehicle and mivebresib treatment groups on day 108. Luminescence/Radiance in p/sec/cm^2/sr.

Transcriptomic changes associated with HDAC and BET inhibition

To elucidate the mechanisms of HDAC and BET inhibition in UM, we performed RNA sequencing on MP41 and MP46 cell lines after 24 h of treatment with drug concentrations that resulted in morphological changes without excessive cell death (40 nM romidepsin, 40 nM quisinostat, and 1200 nM mivebresib). Romidepsin, quisinostat, and mivebresib induced unique morphological changes in MP41 cells, with both HDAC inhibitors causing a flattened morphology, whereas mivebresib-treated cells displayed mixed morphologies with flat and spindle-shaped cells (fig. 4A). Less pronounced effects were observed on the BAP1 mutant MP46 cell line, which presents a heterogenous morphology in culture (supplemental fig. 4A). RNA-seq analysis revealed similar changes in both cell lines, with unique gene expression changes for all three compounds and a clear separation in principle component analysis (PCA) (fig. 4B, 4C; supplemental fig. 4B, 4C). Both HDAC inhibitors resulted in an overall increase in gene expression (fig. 4D; supplemental fig. 4D), which correlates with HDAC inhibitors leading to increased histone acetylation and chromatin accessibility (48). In romidepsin-treated MP41 cells, 2582 genes were significantly upregulated and 1576 were downregulated, whereas in quininostat-treated cells, 1155 genes were significantly upregulated and 374 were downregulated (adjusted P. value < 0.05, Log > |1.5|) (fig. 4D). Most gene expression changes in quininostat-treated cells overlapped with those observed in romidepsin-

treated cells. However, although romidepsin only inhibits class I HDACs, it caused more gene expression changes at the same treatment concentration (40 nM) (fig. 4D, 4E; supplemental fig. 4D, 4E). BET inhibitors prevent the binding of bromodomain (BRD) proteins to acetylated histones, which typically initiate transcription by recruiting transcriptional machinery to acetylated sites (49, 50). In concordance, mivebresib treatment resulted in fewer upregulated genes (n = 885) and more downregulated genes (n = 1464) in MP41 cells (fig. 4D, 4E). Despite their different targets and unique gene expression changes, we found a significant overlap in gene expression changes elicited by HDAC and BET inhibitors (fig. 4D, supplemental fig. 4D). Strikingly, integrated Network-based Cellular Signature (iLINCS) (25) analysis showed that mivebresib treatment causes a gene expression shift that is most similar to various HDAC inhibitors (fig. 4E, 4F; supplemental fig. 4E, 4F).

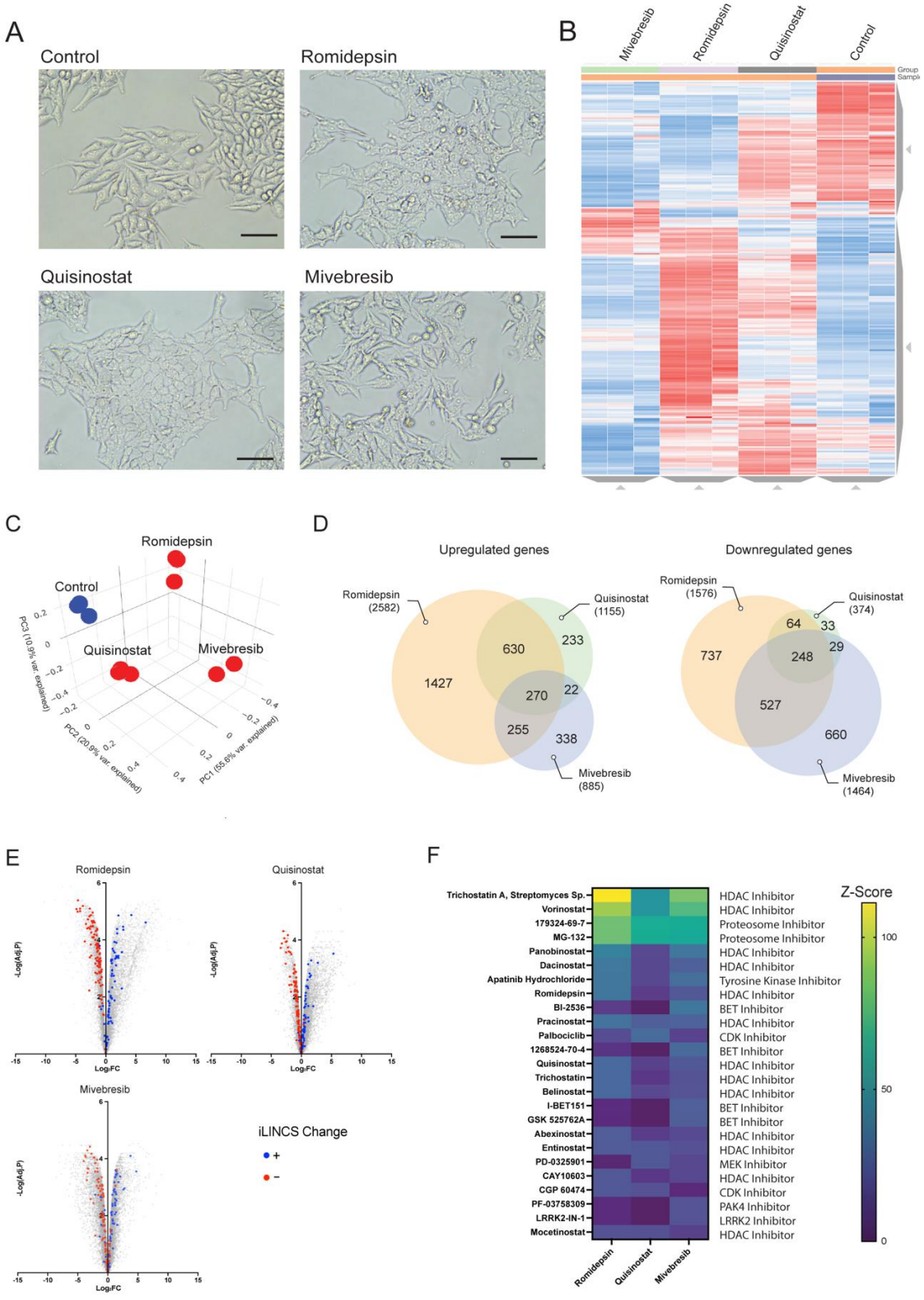

Figure 4. RNA-seq analysis of MP41 cells treated with candidate compounds for 24 h. (A) Images of MP41 cells treated with each compound for 24 hours. Scale bar = 100 µm. **(B)** Heatmap clustering of changes in gene expression per treatment group (n = 3 per condition). **(C)** PCA clustering of replicates for each treatment. **(D)** Venn diagram depicting overlaps between the treatment groups of significantly upregulated and downregulated genes (Adj. $P < 0.05$, $\log_2 FC > |1.5|$). **(E)** Volcano plot of changes in gene expression relative to the control for each treatment group. Blue and red dots are 180 genes found to be consistently dysregulated as a result of eight HDAC inhibitor treatments in iLINCS. Blue dots are genes that were consistently upregulated by HDAC inhibitor treatment, while red dots are genes that were consistently downregulated. **(F)** Heatmap by Z-score of compounds inducing similar gene expression signatures to romidepsin, quisinostat, and mivebresib using iLINCS connected perturbation analysis.

HDAC and BET inhibition reverse transcriptomic signatures associated with high metastatic risk

Clinically, UM can be accurately stratified into metastatic risk groups, namely class 1 (low-risk) and class 2 (high-risk), using a gene expression panel of 12 genes (51-54). An additional biomarker of high metastatic risk for both class 1 and class 2 UM is the expression of *PRAME* (55-57). We found that treatment of MP41 and MP46 UM cells with HDAC and BET inhibitors reversed class 2 signature genes, with high-risk biomarkers such as *HTR2B* and *PRAME* being downregulated (fig. 5A, 5B). Accordingly, many genes with low expression in class 2 tumors, such as *ROBO1* and *LMCD1,* were upregulated following treatment. Furthermore, we observed the upregulation of several genes associated with neuronal cell identity, including *NEFM* (Neuronal Filament Medium), *SYN1* (Synapsin 1), and *NGFR* (Nerve Growth Factor Receptor (NGFR) (fig. 5C; supplemental fig. 5A). Accordingly, pathway analysis revealed the upregulation of several neuronal pathways following treatments, including synaptic transmission, neuronal projection, action potential, as well as neuronal differentiation and modulation of synaptic transmission pathways (fig. 5D-F; supplemental fig. 5B). We did not observe an upregulation of glial cell markers and found of neural crest and melanocytic identity genes downregulated, including *SOX10*, *MLANA*, and *MITF* (fig. 5C; supplemental fig. 5A). Compared to HDAC inhibitors, BET inhibition activated additional pathways involved in the stress response, including NRF2 signaling (fig. 5F; supplemental fig. 5B). All drug treatments induced downregulation of pathways primarily involving DNA replication, cell growth, and proliferation (supplemental fig. 6).

Together, these data indicate that HDAC and BET inhibition induce a phenotype switch, pushing cells towards a class 1 gene expression signature associated with lower metastatic risk and neuronal cell identity. ChIP Enrichment Analysis (ChEA) (24) showed that in both, MP46 and MP41 cells, the most prominent increase in gene expression following HDAC treatments were targets of the polycomb repressive complex (PRC) 1 (RNF2, BMI1) and PRC2 (SUZ12, EZH2, and cofactors MTF2, JARID2) complexes, indicating a loss of PRC activity (fig. 5I, 5K; supplemental fig. 5E). In MP41 cells, the top differential transcription factor activity for all treatments was FOXM1, whose target genes were significantly downregulated in all treatment groups (fig. 5J). FOXM1 activity is associated with a more aggressive UM phenotype, and silencing FOXM1 in UM cells suppresses UM proliferation, migration, and invasion (58). Other transcription factors whose targets were downregulated in all groups included E2F family members, MYC, and the histone demethylase KDM5B. Although there were no unique transcription factors whose target genes were downregulated by mivebresib in MP41 cells, we found a large group of unique transcription factors whose target genes were upregulated (fig. 5G; supplemental fig. 5C). These factors include retinoic acid receptors RXR and RARβ and their binding partners LXR, PPARγ, and PPARδ (fig. 5I), which regulate pathways involved in neuronal differentiation (59-62). Additionally, mivebresib treatment group exhibited unique stress-related signaling via NRF2, KLF6, and ATF3 (fig. 5G, supplemental fig. 5E).

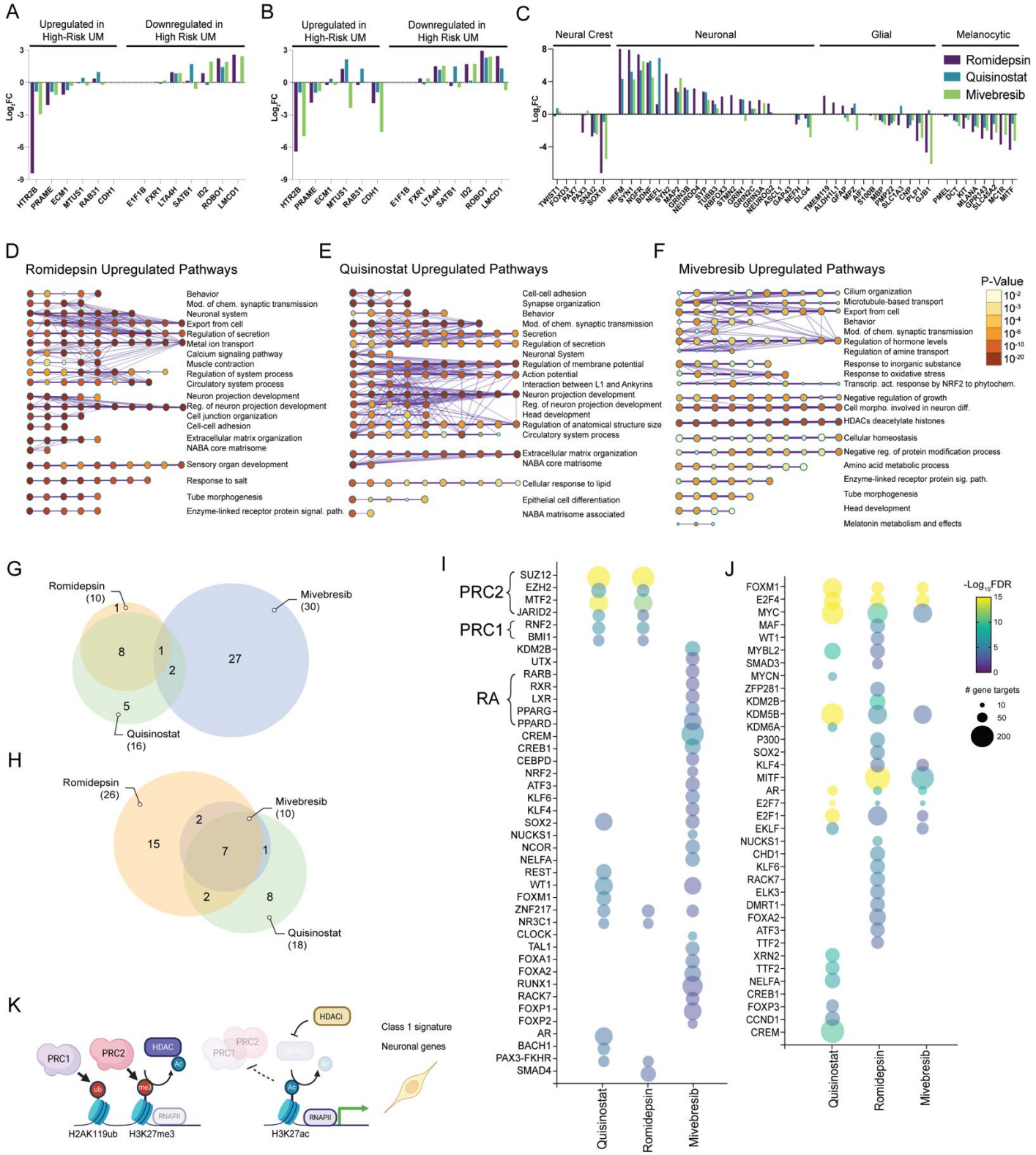

Figure 5. BET and HDAC inhibition act through unique mechanisms with overlapping pathway changes. (A) Changes in the expression (log_2 FC) of genes associated with high- and low-risk UM in drug-treated MP41 cells. **(B)** Changes in the expression (log_2 FC) of genes associated with high- and low-risk UM in drug-treated MP46 cells. **(C)** Changes in the expression (log_2 FC) of genes associated with some neural-crest-derived cell identities in drug-treated MP41 cells. **(D-F)** Gene interaction networks of upregulated pathways in MP41s predicted from significantly upregulated genes in each treatment group (log_2 FC > 1.5, adj. $p < 0.05$). **(G)** Venn diagram showing overlaps in predicted transcription factors with upregulated gene targets in MP41 cells, determined by ChIP-seq data (ChIP Enrichment Analysis (ChEA)). **(H)** Venn diagram showing overlaps in predicted transcription factors with downregulated gene targets in MP41 cells, determined by

ChIP-seq data. **(I)** Bubble plot of the top predicted transcription factors with upregulated targets in MP41 cells for the tested compounds. **(J)** Bubble plot of the top predicted transcription factors with downregulated targets in MP41 cells for the tested compounds. **(K)** Schemetic representation of HDAC inhibition impairing PRC activity, leading to elevated expression of PRC target genes, including neuronal genes and those associated with a class 1 phenotype.

DISCUSSION

The treatment options currently available for metastatic UM are limited, with the most advanced therapies prolonging overall survival by only months for a subset of patients. Here, we present new data utilizing an epigenetic compound screen to identify new vulnerabilities that target the epigenome of UM, as global epigenetic changes correlate with metastatic UM. We show that HDAC and BET inhibitors were the most efficacious compound classes *in vitro*, whereas many other epigenetic modulators, such as histone methyltransferase and PARP inhibitors, did not significantly reduce cell viability. We previously showed that PARP inhibition can reduce the metastatic spread of the MP41 UM cell line in a mouse model of UM (55). However, here our experiments did not identify PARP inhibitors as a potent drug class (fig. 1B, 1C; supplemental fig. 1A), indicating that PARP inhibition acts through other mechanisms than reducing cell viability in this model. HDAC inhibitors have previously been widely considered for UM (37, 41-43), however, with limited clinical success. The class I HDAC inhibitor romidepsin was the most potent compound discovered by our screen *in vitro* ($IC_{50} \approx 3.5$ nM), but it did not improve the survival rate in our metastatic mouse model. Romidepsin is FDA-approved for cutaneous T-cell lymphoma treatment (63) and has been shown to be potent against various other cancer types *in vitro* (64-66). *In vivo* experiments with romidepsin have been challenging in the field, which may be attributed to its short half-life and potential long-term toxicities (67-70). However, its high potency in UM cells highlights class I HDAC inhibition specifically as a potential vulnerability in UM, and may warrant further studies with different treatment paradigms and delivery systems (71-73) to identify an applicable therapeutic window.

We find that the BET inhibitor mivebresib has exceptionally low toxicity towards normal fibroblasts and increased the median survival time from 84 to 121 days in a metastatic UM mouse model. Mivebresib is an oral, small-molecule pan-BET inhibitor that induces cell death and tumor regression in animal models of malignancies such as myeloid leukemia (74), prostate cancer (75), and small cell lung cancer (76). In a clinical trial for patients with solid tumors that included 10 UM patients, mivebresib prevented tumor growth and reduced tumor volumes in a subset of these patients (77). While these results were derived from a small cohort, they highlight, in combination with our findings, that mivebresib treatment may be a clinically feasible option for UM. Remarkably, in our model mivebresib prevented the development of detectable spinal cord and femur metastases. Bone metastasis occurs in approximately 16% of the patients with metastatic UM. While spinal cord metastases are rare (1%), brain metastases are more frequent (5%) (78, 79). Although we did not observe frequent brain metastases in our UM model, the blood-spinal cord barrier (BSCB) is similar to the blood-brain barrier (BBB) in function and morphology, potentially indicating that mivebresib may be able to cross the BSCB/BBB more efficiently than the HDAC inhibitors tested (80-83).

Each compound elicited unique gene expression signatures, however, we identified a significant overlap in the gene expression and pathways deregulated by HDAC and BET inhibition. We found that HDAC inhibition led to the upregulation of PRC1 and PRC2 target genes, whereas BET inhibition acted via other pathways, such as through the upregulation of retinoic acid-related target genes. While promoting cell death, HDAC and BET inhibition both initially caused a phenotypic switch, reversing the clinical class 2 (high-risk) gene expression signature. The specific reversal of these key markers, both up- and downregulated, shows that both drug classes act by initially pushing tumor cells towards a less aggressive class 1 phenotype, rather than being generically toxic. Previous studies have demonstrated that neural progenitor cells treated with HDAC or BET inhibitors favor a neuronal over glial lineage (84-86). We similarly found that genes associated with glial and melanocytic cells were downregulated, while key neuronal genes and pathways were upregulated. This data indicates that given the shared developmental origin of melanocytes and some neuronal cell types from neural crest (87), the stem-like features of UM cells (88) may allow them to be pharmacologically pushed towards a neuronal phenotype.

In summary, our data reveal different mechanisms by which HDAC and BET inhibitors reduce the viability of UM cells. However, overlapping pathways induce a neuronal and lower metastatic risk phenotype. Our results specifically highlight the BET inhibitor mivebresib as a promising candidate for targeting the epigenome of UM to reduce metastatic growth.

Acknowledgements

This work was supported by funds from the Sylvester Comprehensive Cancer Center (SCCC) and Interdisciplinary Stem Cell Institute (ISCI), the American Cancer Society (ACS) Discovery Boost Grant, the Elsa Pardee Foundation, the Sinskey Foundation, and NIH NEI R21EY036185-01 (S.K.). We thank the Cancer Modeling Shared Resource (CMSR, RRID: SCR_022891) from the Sylvester Comprehensive Cancer Center (SCCC) for support with *in vivo* modeling, efficacy studies, noninvasive imaging, and histological work. We thank the Molecular Therapeutic Shared Resource (MTSR) of the SCCC for drug screening support. This work was also supported by funds from 1P30CA240139 of the National Cancer Institute (NCI), the Alcon Research Institute Senior Investigator Award (J.W.H.), and Research to Prevent Blindness, Inc. Senior Scientific Investigator Award (J.W.H.) and Cancer Prevention and Research Institute of Texas Recruitment of Established Investigator Award RR220010 (J.W.H.).

The Bascom Palmer Eye Institute received funding from the National Eye Institute, Grant P30 EY014801, and Research to Prevent Blindness Unrestricted Grant GR004596-1. The Sylvester Comprehensive Cancer Center received funding from the National Cancer Institute (Grant P30 CA240139).

Supplemental Figures

Name	FP41 IC50 (M)	FP38 IC50 (M)	FP46 IC50 (M)	Average IC50 (M)	Mechanism
Alobresib	1.04E-07	1.404E-07	7.122E-08	**1.0514E-07**	BET inhibitor
Podofilox	6.49E-09	1.503E-08	6.562E-09	**9.362E-09**	Topoisomerase II inhibitor
Staurosporine	2.71E-07	5.194E-08	6.863E-07	**3.3648E-07**	PKCα, PKCγ, PKCη inhibitor
SKLB-23bb	8.44E-08	1.742E-05	9.481E-08	**5.86639E-06**	HDAC6 inhibitor
GSK1324726A	1.54E-07	2.475E-07	1.045E-07	**1.68533E-07**	BRD2, BRD3, BRD4 inhibitor
(S)-(+)-Camptothecin	1.17E-07	6.757E-07	2.102E-07	**3.342E-07**	Topoisomerase I inhibitor
Gemcitabine	7.69E-08	1.233E-06	1.686E-07	**4.92843E-07**	DNA synthesis inhibitor
CPI203	1.53E-07	1.604E-07	1.091E-07	**1.40733E-07**	BRD4 inhibitor
NSC228155	2.59E-06	3.216E-07	2.789E-06	**1.90087E-06**	EGFR activator
BET Bromodomain Inhibitor	3.76E-07	3.445E-07	2.477E-07	**3.22667E-07**	BET inhibitor
Panobinostat	1.43E-08	3.575E-08	2.768E-08	**2.58967E-08**	HDAC inhibitor
Quisinostat	9.12E-09	1.162E-08	1.983E-08	**1.35243E-08**	HDAC inhibitor
Fimepinostat	5.96E-09	1.758E-08	9.285E-09	**1.09427E-08**	HDAC and PI3K inhibitor
Cucurbitacin B	4.84E-08	1.41E-08	5.111E-08	**3.78567E-08**	PI3K/AKT inhibitor
Romidepsin	3.16E-14	8.916E-10	1.269E-09	**7.20211E-10**	Class I HDAC inhibitor
AZD5153	9.04E-08	8.867E-08	6.833E-08	**8.24767E-08**	BRD4 inhibitor
Mivebresib	9.96E-08	1.877E-07	8.921E-08	**1.2549E-07**	BET inhibitor
ABBV-744	8.127	2834	0.05655	**947.3945167**	BRD4 inhibitor
Quisinostat 2HCl	5.42E-09	6.754E-09	1.385E-08	**8.674E-09**	HDAC inhibitor
666-15	5.89E-05	0.0005853	0.002194	**0.00094607**	EGFR inhibitor
Velcade	4.34E-09	1.487E-08	3.519E-09	**7.57633E-09**	Proteosome inhibitor

Supplemental Table 1. Primary screen results. IC_{50} (M) values of the hit compounds identified by the primary screen for each UM cell line, along with the mechanism of action of each compound.

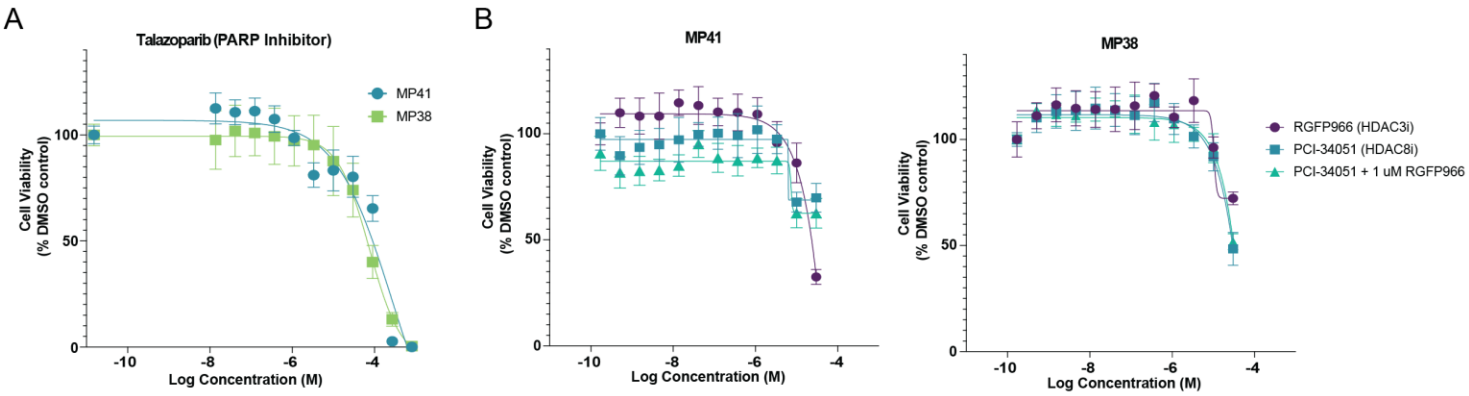

Supplemental Figure 1. PARP inhibitor, HDAC3 inhibitor, and HDAC8 inhibitor concentration-response testing. (A) Concentration-response curves of MP41 and MP38 cells treated with the PARP inhibitor talazoparib. **(B)** Concentration-response curves of MP41 and MP38 cells treated with HDAC3 and HDAC8 inhibitors. N = 4 for each concentration.

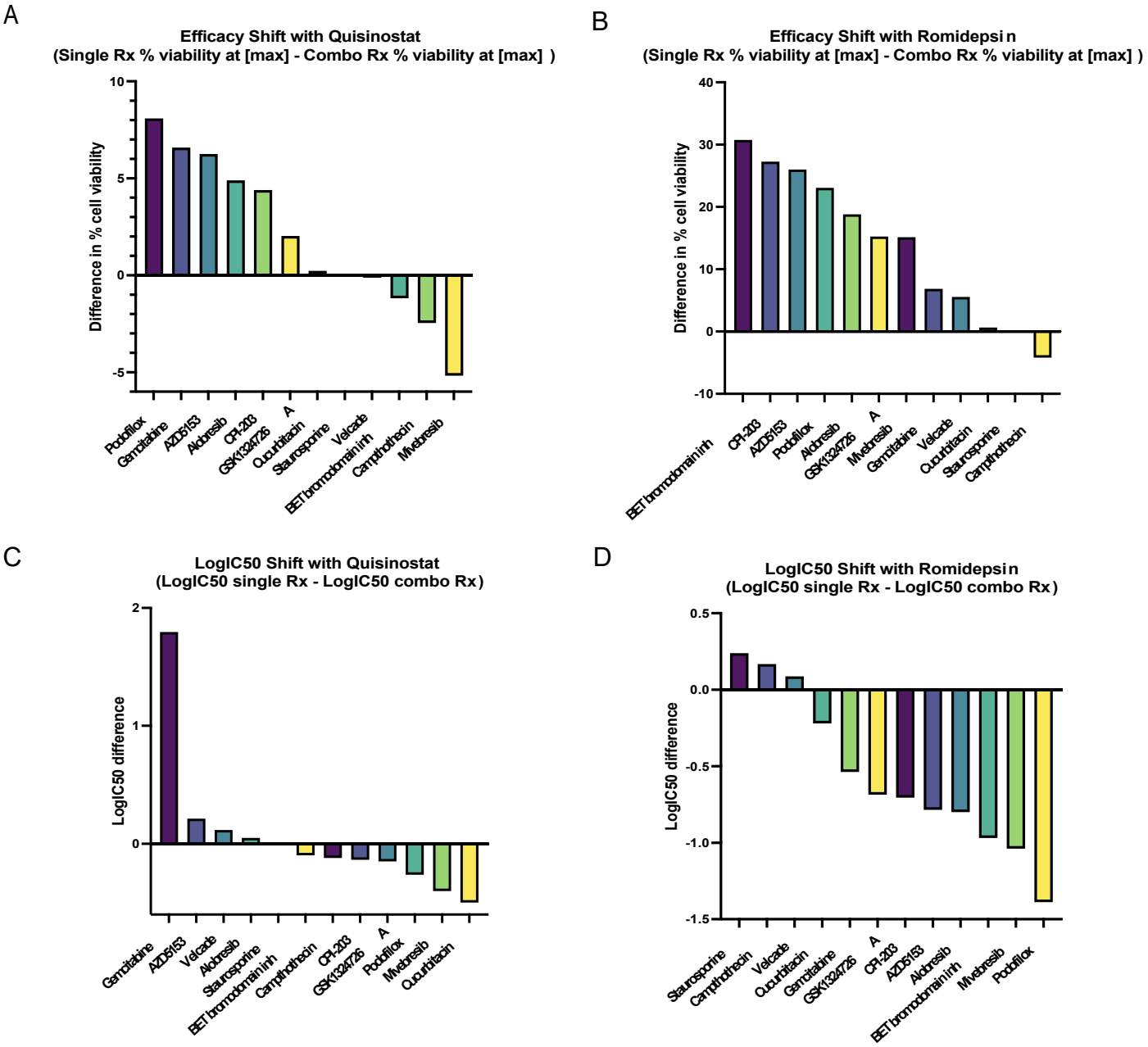

Supplemental Figure 2. Synergistic tests of quisinostat and romidepsin with other candidate compounds. **(A)** Difference in percent cell viability at the highest concentration (10 μM) for cells treated with quisinostat plus EC_{20} of other candidate compound relative to cell viability when treated with only 10 μM quisinostat. Greater positive values indicate better synergy. **(B)** Difference in percent cell viability at the highest concentration (10 μM) for cells treated with romidepsin plus EC_{20} of other candidate compounds relative to cell viability when treated with only 10 μM romidepsin. Greater positive values indicate better synergy. **(C)** Log IC_{50} shift of cells treated with Quisinostat and the EC_{20} of other candidate compounds relative to cells treated with only quisinostat. Greater positive values indicate better synergy. **(D)** Log IC_{50} shift of cells treated with romidepsin and the EC_{20} of other candidate compound relative to cells treated with only romidepsin. Greater positive values indicate better synergy.

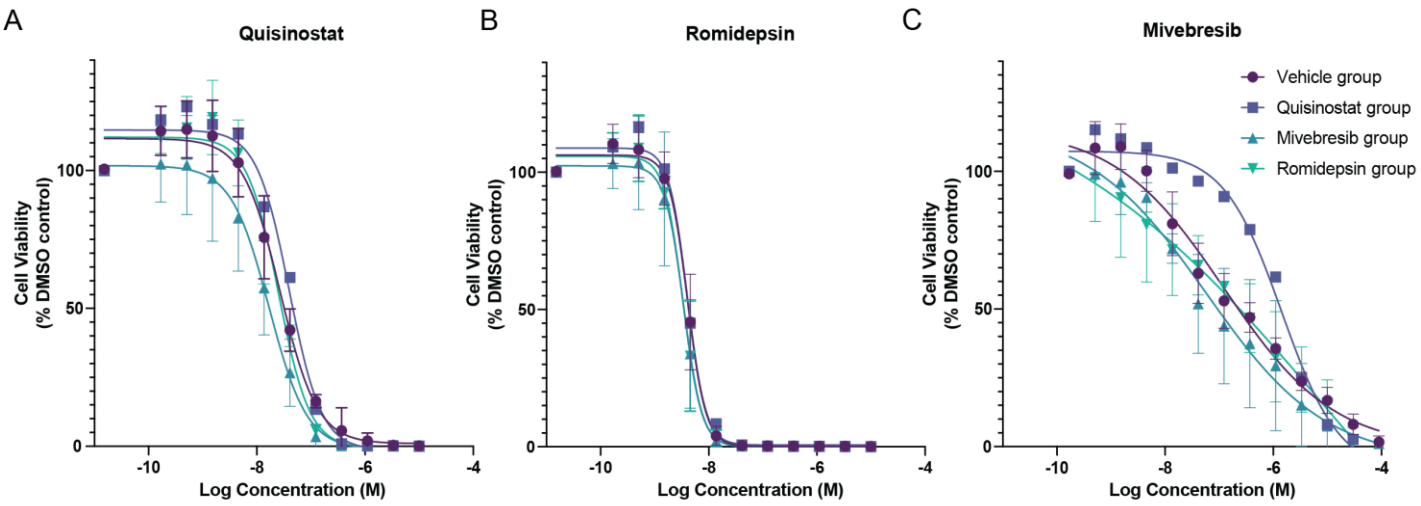

Supplemental Figure 3. *Ex vivo* testing of acquired drug resistance in vehicle-and treated tumor cells from murine livers. (A) Concentration-response curve of quisinostat treatment of MP41 cells extracted from mouse liver tumor samples averaged for each treatment group (vehicle n =3; quisinostat n =1, mivebresib n = 4, romidepsin n = 3). **(B**) Concentration-response curve of romidepsin treatment of MP41 cells extracted from mouse liver tumor samples averaged for each treatment group. **(C)** Concentration-response curve of mivebresib treatment of MP41 cells extracted from mouse liver tumor samples averaged for each treatment group.

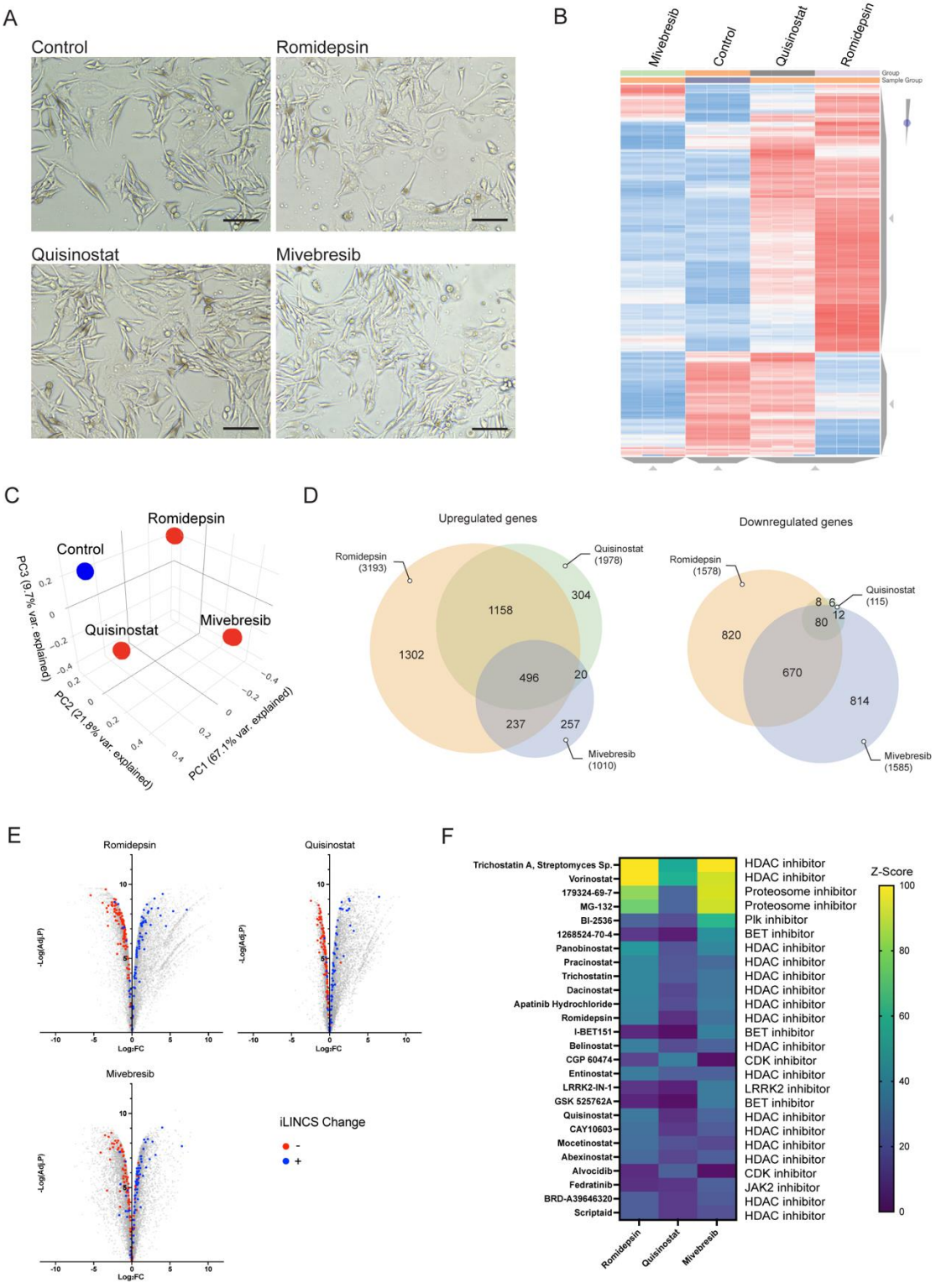

Supplemental Figure 4. RNA-seq analysis of MP46 cells treated with candidate compounds for 24 h. (A) Images of MP46 cells treated with each compound for 24 hours. Scale bar = 100 µm. **(B)** Heatmap clustering of changes in gene expression of MP46 cells per treatment group (n = 3 per condition). **(C)** PCA clustering of replicates for each treatment in MP46 cells. **(D)** Venn diagram depicting overlaps between the treatment groups of significantly upregulated and downregulated genes in drug-treated MP46 cells. **(E)** Volcano plot of changes in gene expression relative to the control for each treatment group in MP46 cells. Blue and red dots are 180 genes found to be consistently dysregulated as a result of eight HDAC inhibitor treatments in iLINCS. Blue dots are genes that were consistently upregulated by HDAC inhibitor treatment, while red dots are genes that were consistently downregulated. **(F)** Heatmap of perturbations inducing similar gene expression signatures to romidepsin, quisinostat, and mivebresib in MP46s using iLINCS connected perturbation analysis.

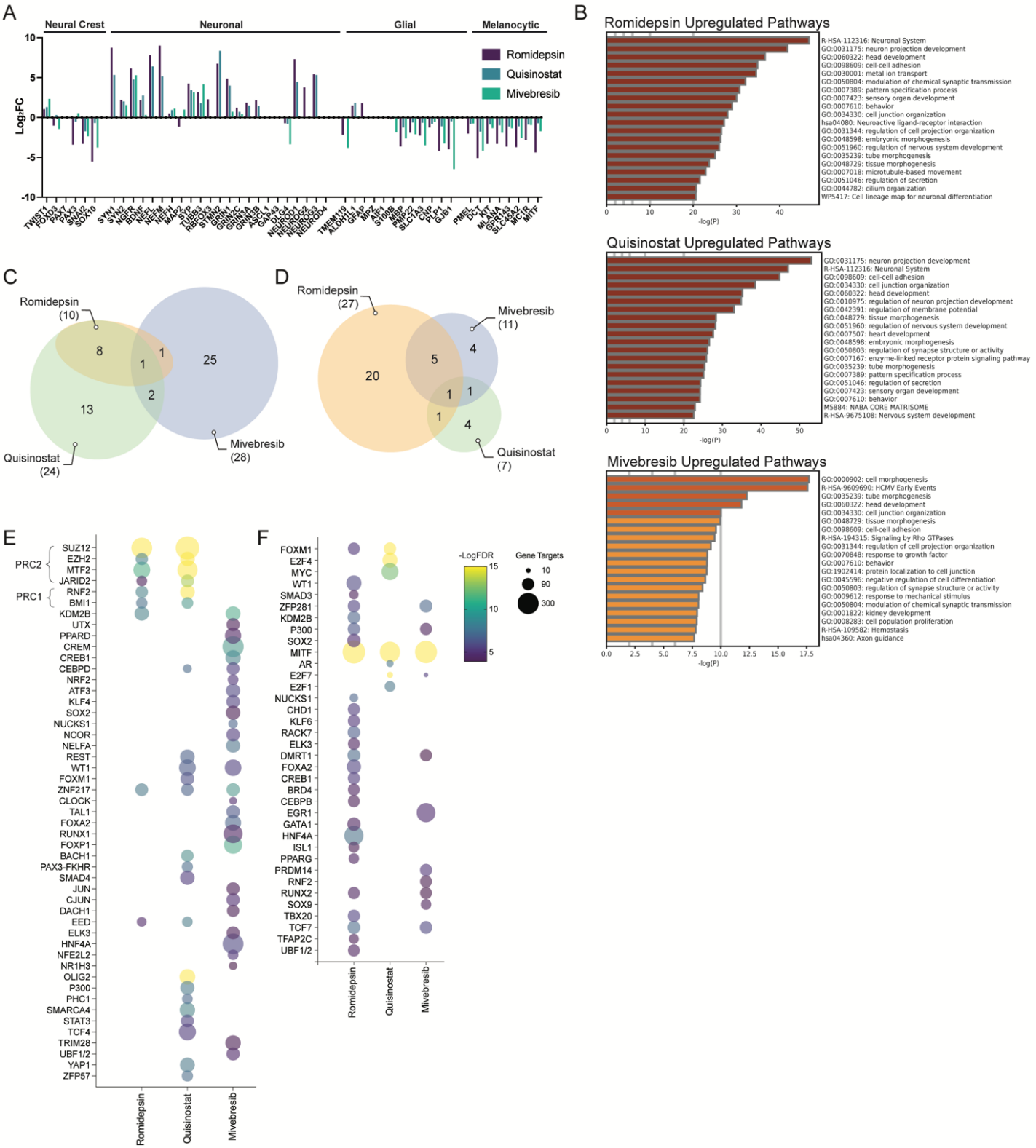

Supplemental Figure 5. BET and HDAC inhibition mechanisms and pathway changes in MP46 cells. (A) Changes in the expression (log_2 FC) of genes associated with some neural-crest-derived cell identities in drug-treated MP46 cells. **(B)** Upregulated pathways in drug-treated MP46 cells predicted from list of significantly upregulated genes in each treatment group (log_2 FC > 1.5, adj. $p < 0.05$). **(C)** Venn diagram showing overlaps in predicted transcription factors with upregulated gene targets in MP46 cells, determined by ChIP-seq data (ChIP Enrichment Analysis (ChEA)). **(D)** Venn diagram showing overlaps in predicted transcription factors with downregulated gene targets in MP46 cells, determined by ChIP-seq data. **(E)** Bubble plot of the top predicted transcription factors with upregulated targets in MP46 cells for the tested compounds. **(F)** Bubble plot of the top predicted transcription factors with downregulated targets in MP46 cells for the tested compounds.

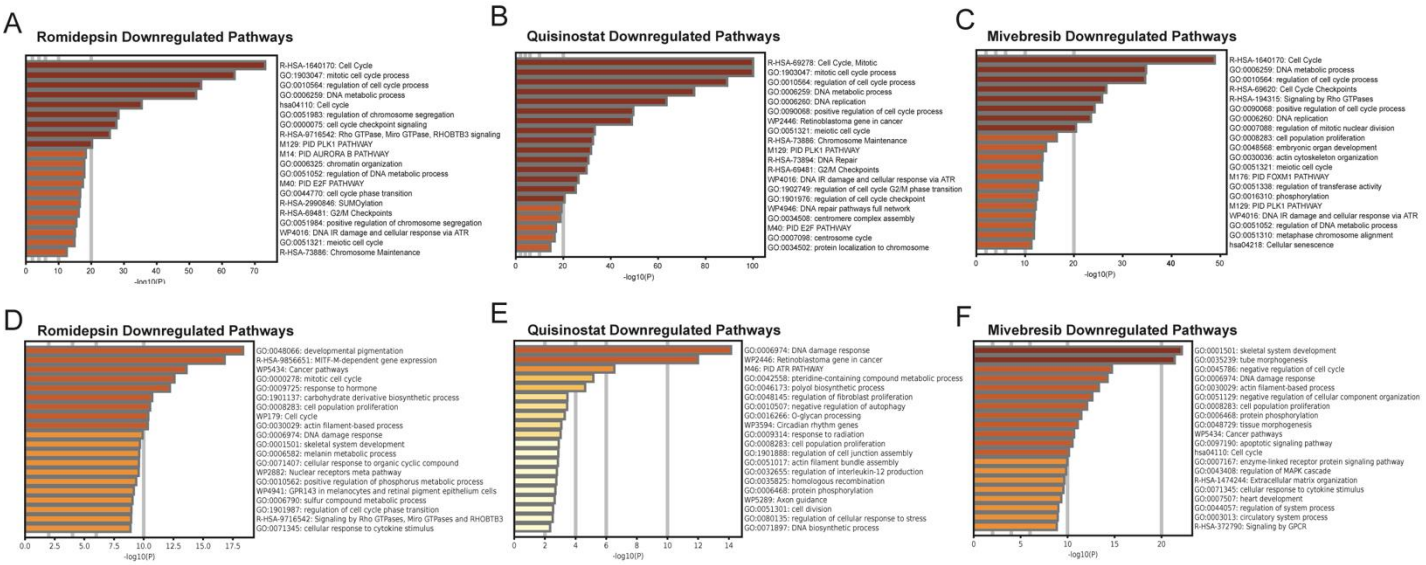

Supplemental Figure 6. Pathways downregulated by each drug in MP41 and MP46 cells. **(A-C)** The top 25 downregulated pathways in each treatment group were determined by Metascape analysis of the significantly downregulated genes in MP41 cells (log_2 FC < -1.5, adj. P value < 0.05). **(D-F)** The top 25 downregulated pathways in each treatment group were determined by Metascape analysis of the significantly downregulated genes in MP46 cells (log_2 FC < -1.5, adj. P value < 0.05).

References

1. Carvajal RD, Sacco JJ, Jager MJ, Eschelman DJ, Olofsson Bagge R, Harbour JW, et al. Advances in the clinical management of uveal melanoma. Nature Reviews Clinical Oncology. 2023;20(2):99-115.
2. Nathan P, Hassel JC, Rutkowski P, Baurain J-F, Butler MO, Schlaak M, et al. Overall survival benefit with tebentafusp in metastatic uveal melanoma. New England Journal of Medicine. 2021;385(13):1196-206.
3. Decatur CL, Ong E, Garg N, Anbunathan H, Bowcock AM, Field MG, et al. Driver mutations in uveal melanoma: associations with gene expression profile and patient outcomes. JAMA ophthalmology. 2016;134(7):728-33.
4. Van Raamsdonk CD, Bezrookove V, Green G, Bauer J, Gaugler L, O'Brien JM, et al. Frequent somatic mutations of GNAQ in uveal melanoma and blue naevi. Nature. 2009;457(7229):599-602.
5. Van Raamsdonk CD, Griewank KG, Crosby MB, Garrido MC, Vemula S, Wiesner T, et al. Mutations in GNA11 in uveal melanoma. New England Journal of Medicine. 2010;363(23):2191-9.
6. Johansson P, Aoude LG, Wadt K, Glasson WJ, Warrier SK, Hewitt AW, et al. Deep sequencing of uveal melanoma identifies a recurrent mutation in PLCB4. Oncotarget. 2016;7(4):4624.
7. Moore AR, Ceraudo E, Sher JJ, Guan Y, Shoushtari AN, Chang MT, et al. Recurrent activating mutations of G-protein-coupled receptor CYSLTR2 in uveal melanoma. Nature genetics. 2016;48(6):675-80.
8. Onken MD, Worley LA, Long MD, Duan S, Council ML, Bowcock AM, et al. Oncogenic Mutations in GNAQ Occur Early in Uveal Melanoma. Investigative Opthalmology & Visual Science. 2008;49(12):5230.
9. Vader M, Madigan M, Versluis M, Suleiman H, Gezgin G, Gruis NA, et al. GNAQ and GNA11 mutations and downstream YAP activation in choroidal nevi. British journal of cancer. 2017;117(6):884-7.
10. Harbour JWO, Michael D; Roberson, Elisha D O; Duan, Shenghui; Cao, Li; Worley, Lori A; Council, M Laurin; Matatal, Katie A; Helms, Cynthia; Bowcock, Anne M Frequent Mutation of BAP1 in Metastasizing Uveal Melanomas. SCIENCE. 2010;330(6009):1410-3.
11. Harbour JW, Roberson EDO, Anbunathan H, Onken MD, Worley LA, Bowcock AM. Recurrent mutations at codon 625 of the splicing factor SF3B1 in uveal melanoma. Nature Genetics. 2013;45(2):133-5.
12. Martin M, Maßhöfer L, Temming P, Rahmann S, Metz C, Bornfeld N, et al. Exome sequencing identifies recurrent somatic mutations in EIF1AX and SF3B1 in uveal melanoma with disomy 3. Nature genetics. 2013;45(8):933-6.
13. Durante MA, Field MG, Sanchez MI, Covington KR, Decatur CL, Dubovy SR, et al. Genomic evolution of uveal melanoma arising in ocular melanocytosis. Molecular Case Studies. 2019;5(4):a004051.
14. Durante MA, Rodriguez DA, Kurtenbach S, Kuznetsov JN, Sanchez MI, Decatur CL, et al. Single-cell analysis reveals new evolutionary complexity in uveal melanoma. Nature Communications. 2020;11(1).
15. Field MG, Durante MA, Anbunathan H, Cai LZ, Decatur CL, Bowcock AM, et al. Punctuated evolution of canonical genomic aberrations in uveal melanoma. Nature Communications. 2018;9(1).
16. Campagne A, Lee M-K, Zielinski D, Michaud A, Le Corre S, Dingli F, et al. BAP1 complex promotes transcription by opposing PRC1-mediated H2A ubiquitylation. Nature communications. 2019;10(1):348.
17. Yu H, Mashtalir N, Daou S, Hammond-Martel I, Ross J, Sui G, et al. The ubiquitin carboxyl hydrolase BAP1 forms a ternary complex with YY1 and HCF-1 and is a critical regulator of gene expression. Molecular and cellular biology. 2010;30(21):5071-85.
18. Field MK, Jeffim N; Bussies, Parker L; Cai, Louie Z; Alawa, Karam A; Decatur, Christina L; Kurtenbach, Stefan; Harbour, J William. BAP1 Loss Is Associated with DNA Methylomic Repatterning in Highly Aggressive Class 2 Uveal Melanomas. Clinical cancer research. 2019;25(18):5663.
19. Kuznetsov JN, Aguero TH, Owens DA, Kurtenbach S, Field MG, Durante MA, et al. BAP1 regulates epigenetic switch from pluripotency to differentiation in developmental lineages giving rise to BAP1-mutant cancers. Science advances. 2019;5(9):eaax1738.
20. Bakhoum MF, Francis JH, Agustinus A, Earlie EM, Di Bona M, Abramson DH, et al. Loss of polycomb repressive complex 1 activity and chromosomal instability drive uveal melanoma progression. Nature communications. 2021;12(1):5402.
21. Carbone M, Harbour JW, Brugarolas J, Bononi A, Pagano I, Dey A, et al. Biological mechanisms and clinical significance of BAP1 mutations in human cancer. Cancer discovery. 2020;10(8):1103-20.
22. Torre D, Lachmann A, Ma'ayan A. BioJupies: automated generation of interactive notebooks for RNA-Seq data analysis in the cloud. Cell systems. 2018;7(5):556-61. e3.
23. Zhou Y, Zhou B, Pache L, Chang M, Khodabakhshi AH, Tanaseichuk O, et al. Metascape provides a biologist-oriented resource for the analysis of systems-level datasets. Nature communications. 2019;10(1):1523.

24. Lachmann A, Xu H, Krishnan J, Berger SI, Mazloom AR, Ma'ayan A. ChEA: transcription factor regulation inferred from integrating genome-wide ChIP-X experiments. Bioinformatics. 2010;26(19):2438-44.
25. Pilarczyk M, Fazel-Najafabadi M, Kouril M, Shamsaei B, Vasiliauskas J, Niu W, et al. Connecting omics signatures and revealing biological mechanisms with iLINCS. Nature communications. 2022;13(1):4678.
26. Némati F, Sastre-Garau X, Laurent C, Couturier J, Mariani P, Desjardins L, et al. Establishment and characterization of a panel of human uveal melanoma xenografts derived from primary and/or metastatic tumors. Clinical cancer research. 2010;16(8):2352-62.
27. Adams J, Kauffman M. Development of the proteasome inhibitor Velcade™(Bortezomib). Cancer investigation. 2004;22(2):304-11.
28. Ross DD, Cuddy DP. Molecular effects of 2',2'-difluorodeoxycytidine (Gemcitabine) on DNA replication in intact HL-60 cells. Biochem Pharmacol. 1994;48(8):1619-30.
29. Schmittel A, Schmidt-Hieber M, Martus P, Bechrakis N, Schuster R, Siehl J, et al. A randomized phase II trial of gemcitabine plus treosulfan versus treosulfan alone in patients with metastatic uveal melanoma. Annals of oncology. 2006;17(12):1826-9.
30. Tamaoki T, Nomoto H, Takahashi I, Kato Y, Morimoto M, Tomita F. Staurosporine, a potent inhibitor of phospholipidCa++ dependent protein kinase. Biochemical and biophysical research communications. 1986;135(2):397-402.
31. Lapadula D, Farias E, Randolph CE, Purwin TJ, McGrath D, Charpentier TH, et al. Effects of oncogenic Gαq and Gα11 inhibition by FR900359 in uveal melanoma. Molecular Cancer Research. 2019;17(4):963-73.
32. He Y-G, Mayhew E, Mellon J, Niederkorn JY. Expression and possible function of IL-2 and IL-15 receptors on human uveal melanoma cells. Investigative ophthalmology & visual science. 2004;45(12):4240-6.
33. Liu LF, Desai SD, LI TK, Mao Y, Sun M, SIM SP. Mechanism of action of camptothecin. Annals of the New York Academy of Sciences. 2000;922(1):1-10.
34. Gardner TJ, Cohen T, Redmann V, Lau Z, Felsenfeld D, Tortorella D. Development of a high-content screen for the identification of inhibitors directed against the early steps of the cytomegalovirus infectious cycle. Antiviral research. 2015;113:49-61.
35. Garg S, Kaul SC, Wadhwa R. Cucurbitacin B and cancer intervention: Chemistry, biology and mechanisms. International journal of oncology. 2018;52(1):19-37.
36. Landreville SA, Olga A; Matatall, Katie A; Kneass, Zachary T; Onken, Michael D; Lee, Ryan S; Bowcock, Anne M; Harbour, J William. Histone Deacetylase Inhibitors Induce Growth Arrest and Differentiation in Uveal Melanoma. Clinical cancer research. 2012;18(2):408.
37. Kuznetsoff JNO, Dawn A.; Lopez, Andy; Rodriguez, Daniel A.; Chee, Nancy T.; Kurtenbach, Stefan; Bilbao, Daniel; Roberts, Evan R.; Volmar, Claude-Henry; Wahlestedt, Claes; Brothers, Shaun P.; Harbour, J. William. Dual Screen for Efficacy and Toxicity Identifies HDAC Inhibitor with Distinctive Activity Spectrum for BAP1-Mutant Uveal Melanoma. Molecular cancer research. 2021;19(2):215.
38. Sundaramurthi H, García-Mulero S, Tonelotto V, Slater K, Marcone S, Piulats JM, et al. Uveal melanoma cell line proliferation is inhibited by ricolinostat, a histone deacetylase inhibitor. Cancers. 2022;14(3):782.
39. Moschos MM, Dettoraki M, Androudi S, Kalogeropoulos D, Lavaris A, Garmpis N, et al. The role of histone deacetylase inhibitors in uveal melanoma: current evidence. Anticancer research. 2018;38(7):3817-24.
40. Nencetti S, Cuffaro D, Nuti E, Ciccone L, Rossello A, Fabbi M, et al. Identification of histone deacetylase inhibitors with (arylidene) aminoxy scaffold active in uveal melanoma cell lines. Journal of Enzyme Inhibition and Medicinal Chemistry. 2021;36(1):34-47.
41. Wang Y, Liu M, Jin Y, Jiang S, Pan J. In vitro and in vivo anti-uveal melanoma activity of JSL-1, a novel HDAC inhibitor. Cancer letters. 2017;400:47-60.
42. Faião-Flores F, Emmons MF, Durante MA, Kinose F, Saha B, Fang B, et al. HDAC inhibition enhances the in vivo efficacy of MEK inhibitor therapy in uveal melanoma. Clinical Cancer Research. 2019;25(18):5686-701.
43. Dai W, Zhou J, Jin B, Pan J. Class III-specific HDAC inhibitor Tenovin-6 induces apoptosis, suppresses migration and eliminates cancer stem cells in uveal melanoma. Scientific reports. 2016;6(1):22622.
44. Winter M, Moser MA, Meunier D, Fischer C, Machat G, Mattes K, et al. Divergent roles of HDAC1 and HDAC2 in the regulation of epidermal development and tumorigenesis. The EMBO Journal. 2013;32(24):3176-91.
45. Nicolas E, Yamada T, Cam HP, FitzGerald PC, Kobayashi R, Grewal SI. Distinct roles of HDAC complexes in promoter silencing, antisense suppression and DNA damage protection. Nature structural & molecular biology. 2007;14(5):372-80.

46. Witt O, Deubzer HE, Milde T, Oehme I. HDAC family: What are the cancer relevant targets? Cancer letters. 2009;277(1):8-21.
47. Gentien D, Saberi-Ansari E, Servant N, Jolly A, de la Grange P, Némati F, et al. Multi-omics comparison of malignant and normal uveal melanocytes reveals molecular features of uveal melanoma. Cell reports. 2023;42(9).
48. Slaughter MJ, Shanle EK, Khan A, Chua KF, Hong T, Boxer LD, et al. HDAC inhibition results in widespread alteration of the histone acetylation landscape and BRD4 targeting to gene bodies. Cell reports. 2021;34(3).
49. Dhalluin C, Carlson JE, Zeng L, He C, Aggarwal AK, Zhou M-M, et al. Structure and ligand of a histone acetyltransferase bromodomain. Nature. 1999;399(6735):491-6.
50. Yang Z, Yik JH, Chen R, He N, Jang MK, Ozato K, et al. Recruitment of P-TEFb for stimulation of transcriptional elongation by the bromodomain protein Brd4. Molecular cell. 2005;19(4):535-45.
51. Onken MD, Worley LA, Ehlers JP, Harbour JW. Gene expression profiling in uveal melanoma reveals two molecular classes and predicts metastatic death. Cancer research. 2004;64(20):7205-9.
52. Harbour JW. A prognostic test to predict the risk of metastasis in uveal melanoma based on a 15-gene expression profile. Molecular Diagnostics for Melanoma: Methods and Protocols. 2014:427-40.
53. Cai L, Paez-Escamilla M, Walter SD, Tarlan B, Decatur CL, Perez BM, et al. Gene expression profiling and PRAME status versus tumor-node-metastasis staging for prognostication in uveal melanoma. American journal of ophthalmology. 2018;195:154-60.
54. Harbour JW, Chen R. The DecisionDx-UM gene expression profile test provides risk stratification and individualized patient care in uveal melanoma. PLoS currents. 2013;5.
55. Kurtenbach S, Sanchez MI, Kuznetsoff J, Rodriguez DA, Weich N, Dollar JJ, et al. PRAME induces genomic instability in uveal melanoma. Oncogene. 2023:1-11.
56. Field MG, Decatur CL, Kurtenbach S, Gezgin G, Van Der Velden PA, Jager MJ, et al. PRAME as an independent biomarker for metastasis in uveal melanoma. Clinical cancer research. 2016;22(5):1234-42.
57. Harbour JW, Correa ZM, Schefler AC, Mruthyunjaya P, Materin MA, Aaberg TA, Jr., et al. 15-Gene Expression Profile and PRAME as Integrated Prognostic Test for Uveal Melanoma: First Report of Collaborative Ocular Oncology Group Study No. 2 (COOG2.1). J Clin Oncol. 2024:JCO2400447.
58. Bai X, Li S, Luo Y. FOXM1 promote the growth and metastasis of uveal melanoma cells by regulating CDK2 expression. International Ophthalmology. 2024;44(1):55.
59. Yu S, Levi L, Siegel R, Noy N. Retinoic acid induces neurogenesis by activating both retinoic acid receptors (RARs) and peroxisome proliferator-activated receptor β/δ (PPARβ/δ). Journal of Biological Chemistry. 2012;287(50):42195-205.
60. Quintanilla RA, Utreras E, Cabezas-Opazo FA. Role of PPARγ in the Differentiation and Function of Neurons. PPAR research. 2014;2014(1):768594.
61. Simandi Z, Horvath A, Cuaranta-Monroy I, Sauer S, Deleuze J-F, Nagy L. RXR heterodimers orchestrate transcriptional control of neurogenesis and cell fate specification. Molecular and cellular endocrinology. 2018;471:51-62.
62. Schmidt A, Vogel R, Holloway MK, Rutledge SJ, Friedman O, Yang Z, et al. Transcription control and neuronal differentiation by agents that activate the LXR nuclear receptor family. Molecular and cellular endocrinology. 1999;155(1-2):51-60.
63. VanderMolen KM, McCulloch W, Pearce CJ, Oberlies NH. Romidepsin (Istodax, NSC 630176, FR901228, FK228, depsipeptide): a natural product recently approved for cutaneous T-cell lymphoma. The Journal of antibiotics. 2011;64(8):525-31.
64. Mayr C, Kiesslich T, Erber S, Bekric D, Dobias H, Beyreis M, et al. HDAC screening identifies the HDAC class I inhibitor romidepsin as a promising epigenetic drug for biliary tract cancer. Cancers. 2021;13(15):3862.
65. Panicker J, Li Z, McMahon C, Sizer C, Steadman K, Piekarz R, et al. Romidepsin (FK228/depsipeptide) controls growth and induces apoptosis in neuroblastoma tumor cells. Cell cycle. 2010;9(9):1830-8.
66. Li L-H, Zhang P-R, Cai P-Y, Li Z-C. Histone deacetylase inhibitor, Romidepsin (FK228) inhibits endometrial cancer cell growth through augmentation of p53-p21 pathway. Biomedicine & Pharmacotherapy. 2016;82:161-6.
67. Rivers ZT, Oostra DR, Westholder JS, Vercellotti GM. Romidepsin-associated cardiac toxicity and ECG changes: A case report and review of the literature. Journal of Oncology Pharmacy Practice. 2018;24(1):56-62.

68. Klimek VM, Fircanis S, Maslak P, Guernah I, Baum M, Wu N, et al. Tolerability, pharmacodynamics, and pharmacokinetics studies of depsipeptide (romidepsin) in patients with acute myelogenous leukemia or advanced myelodysplastic syndromes. Clinical Cancer Research. 2008;14(3):826-32.
69. Woo S, Gardner ER, Chen X, Ockers SB, Baum CE, Sissung TM, et al. Population pharmacokinetics of romidepsin in patients with cutaneous T-cell lymphoma and relapsed peripheral T-cell lymphoma. Clinical cancer research. 2009;15(4):1496-503.
70. Byrd JC, Marcucci G, Parthun MR, Xiao JJ, Klisovic RB, Moran M, et al. A phase 1 and pharmacodynamic study of depsipeptide (FK228) in chronic lymphocytic leukemia and acute myeloid leukemia. Blood. 2005;105(3):959-67.
71. Pal I, Illendula A, Manavalan JS, Fox TP, O'Connor OA, Loughran TP, et al. The Novel Nano-Formulation of the HDAC Inhibitor, Romidepsin, for the Treatment of Relapsed, Refractory Peripheral T-Cell Lymphoma. Blood. 2022;140(Supplement 1):8848-9.
72. Wang EC, Min Y, Palm RC, Fiordalisi JJ, Wagner KT, Hyder N, et al. Nanoparticle formulations of histone deacetylase inhibitors for effective chemoradiotherapy in solid tumors. Biomaterials. 2015;51:208-15.
73. Lindemann H, Kühne M, Grune C, Warncke P, Hofmann S, Koschella A, et al. Polysaccharide nanoparticles bearing HDAC inhibitor as nontoxic nanocarrier for drug delivery. Macromolecular Bioscience. 2020;20(6):2000039.
74. Albert DH, Goodwin NC, Davies AM, Rowe J, Feuer G, Boyiadzis M, et al. Co-clinical modeling of the activity of the BET inhibitor mivebresib (ABBV-075) in AML. in vivo. 2022;36(4):1615-27.
75. Faivre EJ, Wilcox D, Lin X, Hessler P, Torrent M, He W, et al. Exploitation of castration-resistant prostate cancer transcription factor dependencies by the novel BET inhibitor ABBV-075. Molecular Cancer Research. 2017;15(1):35-44.
76. Lam LT, Lin X, Faivre EJ, Yang Z, Huang X, Wilcox DM, et al. Vulnerability of small-cell lung cancer to apoptosis induced by the combination of BET bromodomain proteins and BCL2 inhibitors. Molecular cancer therapeutics. 2017;16(8):1511-20.
77. Piha-Paul SA, Sachdev JC, Barve M, LoRusso P, Szmulewitz R, Patel SP, et al. First-in-human study of mivebresib (ABBV-075), an oral pan-inhibitor of bromodomain and extra terminal proteins, in patients with relapsed/refractory solid tumors. Clinical Cancer Research. 2019;25(21):6309-19.
78. Group TCOMS. Assessment of Metastatic Disease Status at Death in 435 Patients With Large Choroidal Melanoma in the Collaborative Ocular Melanoma Study (COMS): COMS Report No. 15. Archives of Ophthalmology. 2001;119(5):670-6.
79. Wei AZ, Uriel M, Porcu A, Manos MP, Mercurio AC, Caplan MM, et al. Characterizing metastatic uveal melanoma patients who develop symptomatic brain metastases. Frontiers in Oncology. 2022;12:961517.
80. Jermakowicz AM, Rybin MJ, Suter RK, Sarkaria JN, Zeier Z, Feng Y, et al. The novel BET inhibitor UM-002 reduces glioblastoma cell proliferation and invasion. Scientific reports. 2021;11(1):23370.
81. Bai P, Lan Y, Patnaik D, Wang H, Liu Y, Chen Z, et al. Design, synthesis, and evaluation of thienodiazepine derivatives as positron emission tomography imaging probes for bromodomain and extra-terminal domain family proteins. Journal of Medicinal Chemistry. 2021;64(19):14745-56.
82. Sullivan JM, Badimon A, Schaefer U, Ayata P, Gray J, Chung C-w, et al. Autism-like syndrome is induced by pharmacological suppression of BET proteins in young mice. Journal of Experimental Medicine. 2015;212(11):1771-81.
83. Govindarajan V, Shah AH, Di L, Rivas S, Suter RK, Eichberg DG, et al. Systematic review of epigenetic therapies for treatment of IDH-mutant glioma. World neurosurgery. 2022;162:47-56.
84. Siebzehnrubl FA, Buslei R, Eyupoglu IY, Seufert S, Hahnen E, Blumcke I. Histone deacetylase inhibitors increase neuronal differentiation in adult forebrain precursor cells. Experimental Brain Research. 2007;176:672-8.
85. Hsieh J, Nakashima K, Kuwabara T, Mejia E, Gage FH. Histone deacetylase inhibition-mediated neuronal differentiation of multipotent adult neural progenitor cells. Proceedings of the National Academy of Sciences. 2004;101(47):16659-64.
86. Li J, Ma J, Meng G, Lin H, Wu S, Wang J, et al. BET bromodomain inhibition promotes neurogenesis while inhibiting gliogenesis in neural progenitor cells. Stem cell research. 2016;17(2):212-21.
87. Le Douarin N, Kalcheim C. The neural crest: Cambridge university press; 1999.
88. Matatall KA, Agapova OA, Onken MD, Worley LA, Bowcock AM, Harbour JW. BAP1 deficiency causes loss of melanocytic cell identity in uveal melanoma. BMC cancer. 2013;13:1-12.